

Development of Supported Iron Oxide Catalyst for Destruction of PCDD/F

S. LOMNICKI AND B. DELLINGER*

Chemistry Department, Louisiana State University,
232 Choppin Hall, Baton Rouge, Louisiana 70803

Studies on the development of supported iron oxide catalysts for PCDD/F decomposition using 2-monochlorophenol as a surrogate test compound are presented. Iron oxide catalysts supported on titania were prepared by two methods: impregnation and the sol–gel method. The latter preparation method resulted in better dispersion of iron oxide on the surface and the formation of γ -Fe₂O₃. This is in contrast to the impregnated samples where α -Fe₂O₃ crystallites were formed. Formation of γ -Fe₂O₃ resulted in improved reducibility of the active phase that favorably affected the catalytic oxidation properties of the catalyst, i.e., the light-off curves for the sol–gel samples were shifted toward lower temperature. Addition of calcium oxide to iron oxide catalyst further improved the performance of the system through stabilization and increase in the concentration of γ -Fe₂O₃ in the sol–gel prepared samples. Addition of calcium oxide has a dual effect on the performance of the catalyst. First, it creates oxygen vacancies in the reduction-resistant Fe₂O₃ octahedral structures, thereby improving the reducibility of the active phase. Second, iron oxide can transform during decomposition of chlorinated hydrocarbons into iron chloride. Calcium oxide improved the chlorine transfer from the surface iron oxide species, thereby providing a relatively fresh surface for further catalytic oxidation. Comparison of TPR profiles with the position of light-off curves in 2-monochlorophenol decomposition led to the conclusion that Fe₃O₄ species are the active phase under conditions that facilitate redox cycling between Fe³⁺ and Fe²⁺ ions.

Introduction

Chlorinated organic compounds are a class of pollutants of special concern. Among these, polychlorinated dibenzo-*p*-dioxin and polychlorinated dibenzofurans (PCDD/F) are particularly toxic and dangerous for humans and animals. Unfortunately, their in situ formation accompanies almost every combustion process where a source of chlorine is present. Because of their extreme toxicity, strict emissions standards have been promulgated for PCDD/F emission that limits their concentration to less than 0.20 ng/dscm TEQ (1). TEQ is a toxic equivalent concentration (2), which is calculated based on the toxic equivalency factors (TEF) of various toxic compounds. TEQ is used for a relative measure between different compounds to evaluate remediation and emission. TEQ is a combined effect of different compounds or concentration additive.

* Corresponding author phone: (225)578-9100; fax: (225)678-3458; e-mail: baryyd@lsu.edu.

To meet the standards, exhaust treatment is necessary to remove PCDD/Fs from the stream. Catalytic oxidation/destruction can be an efficient method for PCDD/F removal (3–5). Various oxides have been studied as possible catalysts for PCDD/F decomposition: Cr₂O₃, V₂O₅, MoO₃, Fe₂O₃, Co₃O₄, MnO₂, perovskites, and others (6–8). Recently, there have been reports on the significant effect of calcium oxide and hydroxide on the dechlorination of chlorinated aromatics (9). Interestingly, studies of some oxides such as NiO and Fe₂O₃ supported on CaO indicate that these transition-metal oxides significantly improve the dechlorination properties of CaO as well as improve the oxidative properties (10, 11).

These improvements of catalytic properties are attributed to the ion exchange mechanism between calcium and the transition metal–chlorine ions migrate to calcium and oxygen ligands are transferred to the transition metal. As a result, chlorine atoms adsorbed on transition-metal oxide are transferred into bulk calcium oxide, leaving the active surface relatively unchanged. However, calcium oxide is not a very good support for catalytic systems—it is not hard and excessive emissions of CaO particulates may result in a new type of environmental threat. It is thus interesting to study the effect of doping of supported transition metals with small amounts of calcium oxide. Previous studies indicate that the most significant interface interaction was observed in the Fe₂O₃–CaO system; our studies focus on the development of a supported iron oxide catalyst. Iron oxide-based catalysts can be inexpensive thanks to the abundance of various iron salts. We used titania as a support since our own unpublished data as well as reports by others indicate titania to be the best choice as a support for decomposition of chlorinated compounds (8).

As a surrogate model for PCDD/Fs, we used 2-monochlorophenol (2-MCP). Chlorinated phenols have structures that should behave similar to PCDD/Fs on surfaces in that they both have oxygen and chlorine attached to an aromatic ring. Application of model compounds facilitates sample handling and avoids many of the safety issues associated with PCDD/Fs (5, 7, 8).

Experimental Section

Catalyst Preparation. We prepared a series of catalyst candidates based on titania-supported iron oxides. Some of the catalysts were modified by addition of small amounts of calcium oxide. Two series of catalysts were prepared: impregnated and sol–gel.

Impregnated Samples. Anatase titanium oxide manufactured by Aldrich was used as a support. Iron nitrate nonahydrate (Aldrich) was dissolved in water, and titanium oxide was introduced into the solution. The amount of solution was chosen for the incipient wetness to occur. The suspension was stirred thoroughly for 1 h and dried in an oven at 80 °C for 24 h and at 120 °C for an additional 24 h. Finally, the samples were calcined in air at 450 °C for 12 h. After calcinations, samples were ground and sieved with 100–120 mesh size grain being collected for the catalytic experiments. For the samples doped with calcium oxide, calcium acetylacetonate (Aldrich) was dissolved in the iron nitrate solution prior to introduction of titanium dioxide powder.

Sol–Gel Samples. Active phase precursor (iron(III) acetylacetonate, Aldrich) was dissolved in ethyl alcohol (1:100 by mol). In the case of samples doped with calcium oxide, calcium acetylacetonate was added and dissolved in this

TABLE 1. Characteristics of Prepared Fe₂O₃/TiO₂ Samples

sample symbol	preparation method	iron oxide content (%) ^a	calcium oxide content (%) ^b	surface area (m ² /g)
Ti	Aldrich	0	0	11
TiFe25	impregnation	2.5	0	10
TiFe35	impregnation	3.5	0	15
TiFe50	impregnation	5.0	0	12
TiFe50Ca1	impregnation	5.0	1.0	13
TiFe50Ca3	impregnation	5.0	3.0	11
TiFe50Ca10	impregnation	5.0	10.0	14
SGTiFe25	sol-gel	2.5	0	42
SGTiFe35	sol-gel	3.5	0	59
SGTiFe50	sol-gel	5.0	0	37
SGTiFe25Ca1	sol-gel	2.5	1.0	
SGTiFe25Ca3	sol-gel	2.5	3.0	
SGTiFe25Ca5	sol-gel	2.5	5.0	
SGTiFe50Ca1	sol-gel	5.0	1.0	
SGTiFe50Ca3	sol-gel	5.0	3.0	
SGTiFe50Ca5	sol-gel	5.0	5.0	

^a Weight % of total mass of catalyst. ^b Mole % of introduced active phase (Fe₂O₃).

solution. A few drops of water and hydrochloric acid were added (1:20 by mol). Titanium isopropoxide (Acros Organics) solution was prepared in ethyl alcohol (1:150 by mol). Both solutions were mixed and left for gelation to occur (usually about 2 weeks). After gelation and drying at room temperature for 3 days, samples were dried at 80 °C under vacuum for 24 h followed by calcinations at 450 °C for 12 h. After calcinations, the samples were ground and sieved and 100–120 mesh grain sizes were collected for the catalytic experiments.

Temperature-Programmed Reduction (TPR). The TPR experiments were conducted using a custom-built TPD/TPR system, based on a HP5890 Series II chromatograph, equipped with TCD detector. A high-temperature reactor built into a GC oven is connected on-line with the detector. Prior to experiments, the samples (50 mg) were oxidized in O₂/He flow (20%, 20 cm³/min) for 1 h at 450 °C. The samples were cooled to 50 °C, and TPR was run with a temperature ramp of 10 °C/min in the range of 50–950 °C. A 10% H₂/He (99.9999 purity) mixture was used as a carrier/reacting gas for the reduction process with a flow of 20 cm³/min. ChromPerfect Spirit Software was used for collecting the data from the TCD detector.

Surface Area. The surface areas of the samples were measured using a Quantachrome Autosorb instrument based on a BET measurement of nitrogen adsorption at 77 K. Prior to each experiment, oxidized samples were degassed for 2 h at 200 °C under vacuum.

The abbreviations, compositions, and surface areas of the candidate catalysts are presented in Table 1.

XRD Measurements. A Bruker/Siemens D5000 automated powder X-ray diffractometer with Rietveld analysis software was used for XRD analysis of the samples.

Catalytic Experiments. Catalytic experiments were performed using a packed bed, one-pass, gravitational quartz reactor (1/4 in. i.d.). A 30 mg amount of catalyst diluted with a 30 mg of quartz powder was placed on a quartz wool bed. The reactor was contained in a high-temperature furnace maintained at constant temperature in the range of 275–450 °C. Prior to each experiment, samples were activated in 20% O₂/He flow (20 cm³/min) for 1 h at 450 °C. 2-Monochlorophenol (2-MCP) was introduced into the gas stream by bubbling the helium stream through a saturator kept at room temperature and filled with liquid 2-MCP. The flow of reacting gases (all BOC Edwards O₂, UHP; He, UHP) was controlled using three mass flow controllers (Mc Millan) adjusted to

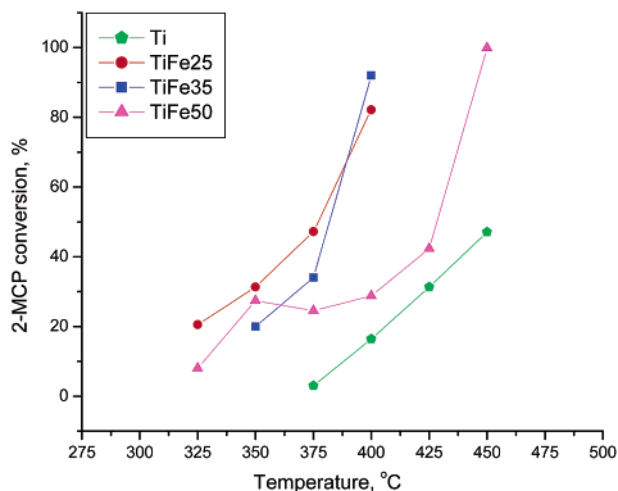


FIGURE 1. 2-MCP conversion over titania and iron oxide supported titania (impregnated samples) as a function of reaction temperature.

maintain 20% O₂ and 15 ppm 2-MCP concentration. Total GHSV equaled 60 000 h⁻¹.

The catalytic reactor was connected in-line with an HP5890 Series II gas chromatograph equipped with flame ionization detector. Sampling of the reaction products as well as bypass reagent was accomplished using a six-port valve equipped with a 2-mL stainless steel loop. The products were separated using Chrompack CP-Sil 8 CB capillary column (30 m, 0.32 mm i.d.). ChromPerfect Spirit Software was used for collecting the data from the GC detector. All transfer lines (stainless steel) were maintained at 180 °C to prevent condensation of heavier products. The tests of the empty reactor as well as the reactor containing the quartz wool bed and quartz powder did not show any conversion of 2-MCP at the studied temperature range. No organic products other than reagents were detected in the exhaust from the reactor for all experiments.

Results

Iron oxide catalyst candidates have been tested with 2-monochlorophenol (2-MCP) decomposition as a surrogate model for their performance for destruction of PCDD/F.

Effect of Iron Oxide Loading. Figure 1 presents the total conversion of 2-MCP for various loadings of catalyst with iron oxide as well as for pure titania. We chose to use titania as a support because it has been previously reported that it is an effective support for destruction of CHCs (4, 8).

As depicted in Figure 1, titania by itself exhibits some activity for destruction of 2-MCP above 400 °C. Impregnation of titania with iron(III) oxide resulted in dramatic improvement in the 2-MCP decomposition. There are significant differences between the particular catalysts with different iron oxide content. The samples with iron oxide in the range of 2.5–3.5% exhibit much better performance with their light-off curves shifted significantly toward (~75 °C) lower temperature than pure titania. Although still better than pure titania, higher iron oxide loadings (5%) resulted in a decrease in activity with respect to lower iron oxide loading. Since the surface area of all the samples is similar (cf. Table 1), the difference in the activity is related to the structure of supported iron oxide species. Indeed, as can be seen on the XRD diffraction pattern of these three samples (cf. Figure 2), higher content of iron oxide results in formation of crystallites of hematite. The lack of the peaks characteristic of crystalline Fe₂O₃ for samples containing 2.5–3.5% iron oxide indicates that better dispersion of the active phase is achieved for these samples.

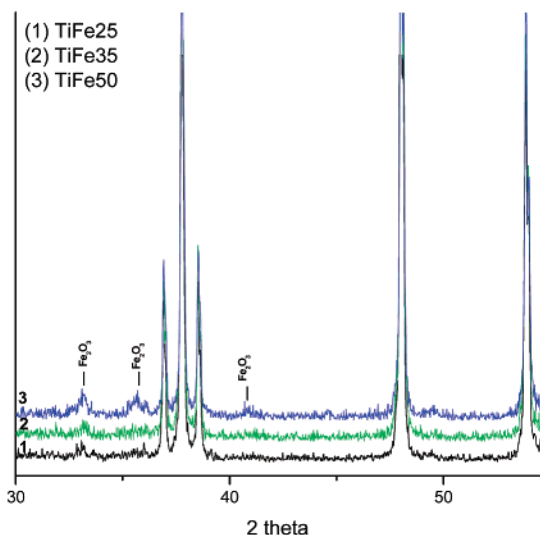


FIGURE 2. XRD spectra of the Fe_2O_3 /titania catalysts (impregnated samples).

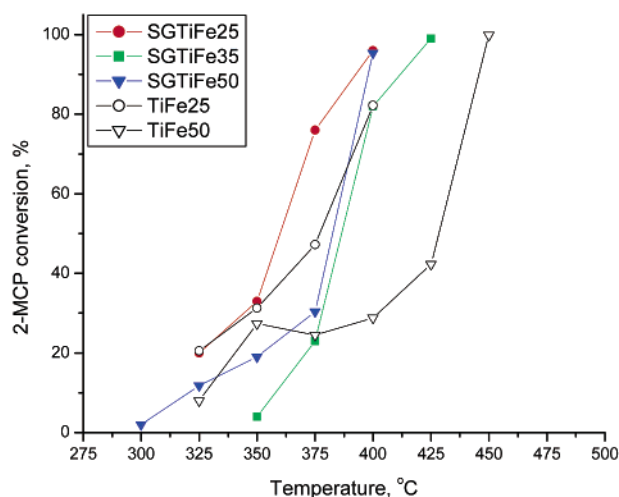


FIGURE 3. Effect of preparation method on 2-MCP destruction ability of Fe_2O_3 titania catalysts.

Effect of Sol–Gel Preparation. To improve the dispersion of the titania-supported iron oxide, we attempted to prepare the catalysts with the sol–gel method. The sol–gel preparation method can sometimes be used to obtain a higher content of active phase without formation of crystalline domains. The SGTiFe catalyst samples were characterized by an increase in surface area (Table 1). The surface area of the SGTiFe catalysts with various iron oxide loadings ranged from 36 to 59 m^2/g , with the highest surface area detected for SGTiFe35 (58.9 m^2/g).

In addition to the surface area, the activity of the catalyst candidates was affected by the preparation method. Figure 3 presents a comparison of the performance of the samples prepared by impregnation and sol–gel methods. The greatest improvement of 2-MCP destruction was observed for the catalysts containing 5% iron oxide, i.e., the light-off curve shifted about 75 °C lower in temperature for the samples prepared by the sol–gel method with respect to similar impregnated sample. The effect of the preparation method on the activity of the samples with low iron oxide content (2.5–3.5%) was less significant; the performance of SGTiFe25 only slightly improved in the temperature range of 375–400 °C (Figure 3), while the performance of SGTiFe35 sample did not change compared to TiFe35 (cf. Figures 1 and 3).

Although the magnitude of improvement is somewhat surprising, it is not entirely unexpected. For lower concen-

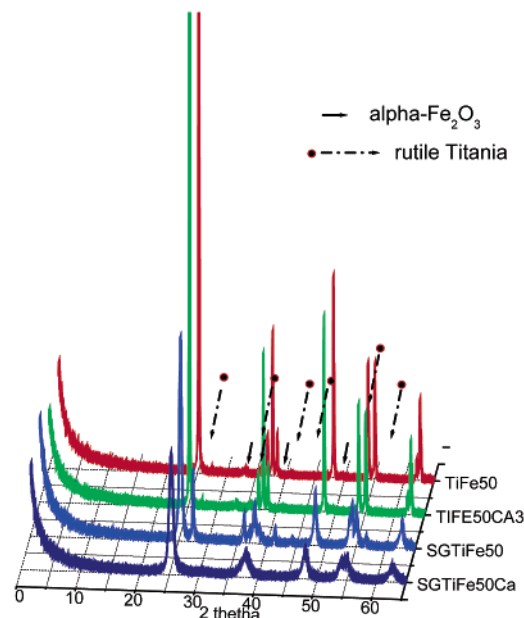


FIGURE 4. Comparison of the XRD spectra of different Fe_2O_3 /titania catalysts.

tration iron oxide impregnated samples, the dispersion of active phase was good and no crystallites of hematite were detected. Consequently, the increase of the surface area for the sol–gel samples did not significantly affect the dispersion. In contrast, for the TiFe50 impregnated catalyst, low dispersion and formation of crystallites of Fe_2O_3 was detected and an increase in surface area for the sol–gel prepared samples should result in improved dispersion of iron oxide species. In fact, the XRD spectrum of the SGTiFe50 catalyst confirms this hypothesis (cf. Figure 4, spectra 1 and 2). Application of sol–gel preparation method resulted in disappearance of the peaks characteristic of $\alpha\text{-Fe}_2\text{O}_3$ crystallites from the samples containing 5% iron oxide, which indicate the lack of larger crystallites with hematite structure.

The differences in the preparation procedure in the sol–gel and impregnation methods may also result in different active phase–support interactions. In the impregnation method, the active phase precursor is deposited on already calcined and formed supports. In contrast, for the sol–gel method, precursors of both support and active phase are well mixed prior to the calcination process and are formed at the same time. This can result in incorporation of the active phase cations in the support structure, which results in a new phase with different properties. XRD spectra of the sol–gel samples did not show the presence of any iron titanates, and the only new peaks detected were those originating from small amounts of rutile titania. The formation of the latter is caused by higher stability of rutile form than the anatase form of titania, the latter tending to transform during calcination into the more thermodynamically stable rutile structure. Since the sol–gel preparation method did not significantly affect other samples than those containing 5% iron oxide, it seems reasonable to conclude that the improvement of the catalytic properties of SGTiFe50 catalyst over TiFe50 is due to improved dispersion of iron oxide phase.

Effect of Calcium Doping. Modification of the supported iron oxide catalyst with calcium was beneficial for the activity of the catalyst in decomposition of 2-MCP. Figure 5 presents the comparison of impregnated TiFe50 samples containing different levels of calcium oxide. Interestingly, smaller amounts of calcium oxide (up to 3%) affected the performance of the catalyst more than higher contents (10%). This clearly

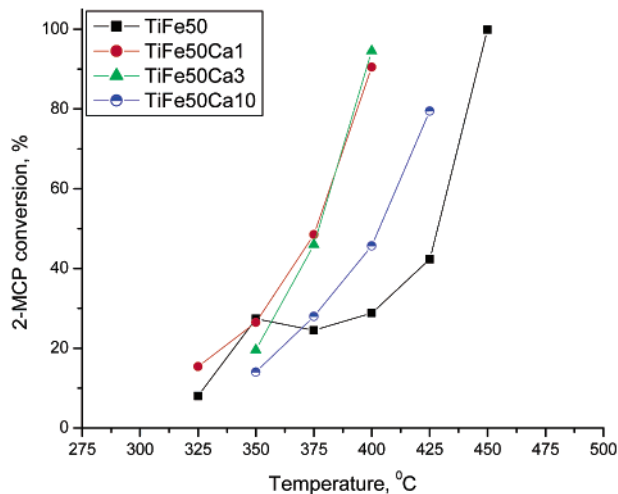


FIGURE 5. Effect of calcium doping on 2-MCP destruction ability of Fe₂O₃/titania catalysts (impregnated samples).

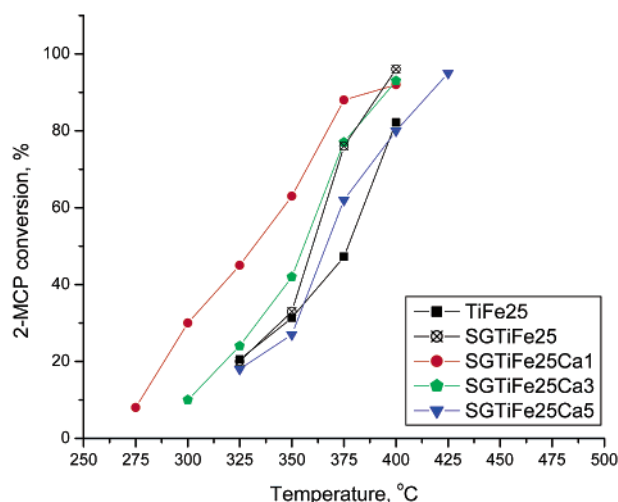


FIGURE 6. Effect of calcium doping on 2-MCP destruction ability of TiFe₂₅ catalysts (sol-gel samples).

indicates a synergistic effect of doping material and not the catalytic activity of calcium oxide alone. (The activity of the CaO/titania samples containing similar amounts of CaO as in the iron oxide/titania doped with calcium catalysts was not different than pure TiO₂) The observed light-off curves shift about 50 °C toward lower temperatures for the TiFe₅₀Ca₁ and TiFe₅₀Ca₃ samples compared to TiFe₅₀ (cf. Figure 5). This temperature shift is similar to what was observed for samples prepared by the sol-gel method (cf. Figure 3). However, in this case, improvement of the catalytic performance of the samples containing calcium oxide could not be explained by the change in the dispersion of iron oxide. The surface area of the samples doped with calcium did not change significantly (Table 1) to force better dispersion of iron oxide species. This is also confirmed by XRD results (Figure 4, spectrum 3), where contrary to SGTiFe₅₀, the lines characteristic of the hematite crystallites in the spectrum of TiFe₅₀Ca₃ were similar to the TiFe₅₀ samples.

Effect of Calcium Doping in Combination with Sol-Gel Preparation. The combination of both sol-gel preparation methods as well as calcium oxide doping resulted in further improvement of the 2-MCP destruction properties of the iron oxide/titania catalyst. Comparisons of the performance of SGTiFe₂₅Ca and SGTiFe₅₀Ca series of catalysts are presented in Figures 6 and 7, respectively. For the SGTiFe₂₅Ca series, the best results were achieved for a very small amount

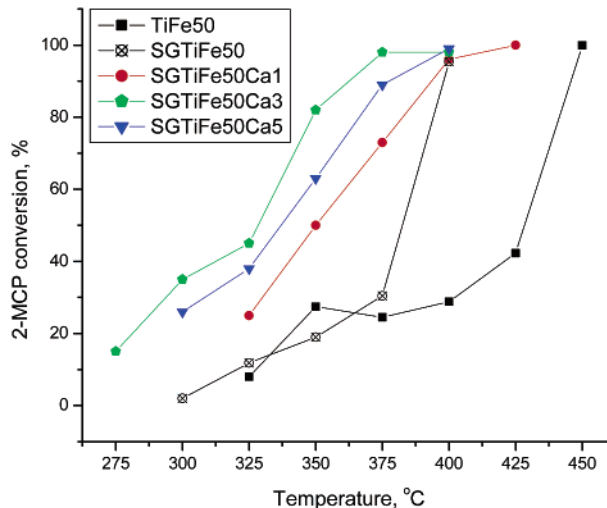


FIGURE 7. Effect of calcium doping on 2-MCP destruction ability of TiFe₅₀ catalysts (sol-gel samples).

of CaO admixture—1% of the active phase. Above this concentration, the light-off curves shifted toward higher temperatures, SGTiFe₂₅Ca₃ demonstrating the same activity as SGTiFe₂₅. Further increase in calcium oxide concentration to 5% resulted in the light-off curve being pushed up to the temperature of the nonmodified TiFe₂₅ catalyst. Nevertheless, the combined effect of preparation method and CaO doping (1%) resulted in significant improvement of the 2-MCP destruction compared to the TiFe₂₅ sample, with a 75 °C shift of activity toward lower temperatures.

The effect of calcium doping together with the sol-gel preparation method is even more profound in the case of the TiFe₅₀ catalyst (cf. Figure 7). The sol-gel preparation method by itself resulted in significant improvement of the 2-MCP decomposition. Addition of calcium oxide allowed further improvement of the activity, with the maximum improvement reached for the SGTiFe₅₀Ca₃ sample. The samples with both higher and lower calcium oxide content appeared to have lower activity, though much better than SGTiFe₅₀.

The application of both calcium doping and sol-gel preparation method affected the structure of the catalyst. The XRD spectrum of the SGTiFe₅₀Ca samples did not show the presence of hematite crystallites, which indicates a good dispersion of iron oxide (cf. Figure 4, spectrum 4). Furthermore, in contrast to the SGTiFe₅₀ sample, the presence of small amounts of calcium oxide prevented the formation of the rutile structure of titania. Moreover, the peaks originating from the anatase form of TiO₂ are much broader compared to other samples, indicating a less ordered material.

Discussion

Oxidation of organics over a surface oxide can occur according to two different mechanisms: the Mars-van Krevelen (MvK) mechanism, which involves the reaction of adsorbed species with exposed surface lattice oxygen, or a bimolecular reaction with gas-phase or adsorbed oxidant (12). Iron oxide catalysts have been reported to catalyze oxidation reactions according to both mechanisms, giving different products of the reaction (13).

2-MCP has been reported to undergo a MvK-type oxidation over a supported copper oxide catalyst (14). The surface of an iron oxide/titania catalyst has been previously found to be oxygen-deficient during the oxidation of methanol (15), which indicates an MvK mechanism. If 2-MCP oxidation on

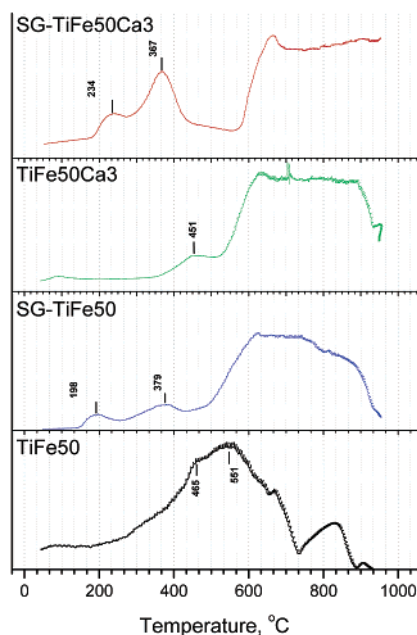


FIGURE 8. TPR profiles of the Fe_2O_3 /titania catalysts.

our supported iron oxide catalyst is also an *MvK* reaction, the destruction of 2-MCP should be related to the reducibility of the iron oxide. Since the reduction properties of supported iron oxides are significantly influenced by its structure and crystallite size (16, 17), better dispersion of the active phase should result in improvement of activity. In fact, application of the sol-gel method of preparation resulted in improved dispersion of the active phase and much better catalytic destruction of 2-MCP (*vide supra*).

Figure 8 presents temperature-programmed reduction (TPR) profiles of our catalyst candidates. The observed peaks correspond to the transformation of $\text{Fe(III)}_2\text{O}_3$ to lower oxidation state iron oxides and iron. Application of the sol-gel method significantly shifts the reduction peaks to lower temperatures compared to the impregnated samples, with the first two TPR peaks appearing at 198 and 379 °C. Since the shift of these two peaks is so great, it is difficult to conclusively identify the type of iron oxide transformation related with a particular peak. Generally, Fe_2O_3 TPR profile peaks are attributed to the transformations of $\text{Fe(III)}_2\text{O}_3 \rightarrow \text{Fe(III,II)}_3\text{O}_4 \rightarrow \text{Fe(II)}\text{O} \rightarrow \text{Fe}^0$ (17–20). However, the reduction peaks observed for SGTiFe are at much lower temperatures. The lowest temperature for a TPR peak for iron oxide was reported to be at 295 °C, although the authors attributed it to undecomposed precursor rather than a reduced iron oxide species (20) due to low-temperature pretreatment conditions. Since all our samples were pre-calcined at 450 °C in air, this seems to be an unlikely scenario for our catalysts.

The XRD spectrum of the SGTiFe samples did not exhibit peaks characteristic of any crystalline iron oxide structure, which suggests that the surface species are two-dimensional. Crystallites of $\alpha\text{-Fe}_2\text{O}_3$ are very difficult to reduce to coordinatively unsaturated ions because of their high geometrical stability of $[\text{FeO}_6]$ octahedral units (21), and the titania surface forces the formation octahedral structures (22). However, it has also been previously reported (23) that the sol-gel preparation method may favor formation of $\gamma\text{-Fe}_2\text{O}_3$ (maghemite), which will not be visible in the XRD spectrum if the crystallites are smaller than 5 nm. $\gamma\text{-Fe}_2\text{O}_3$ has a cubic, spinel structure with the cationic vacancies and iron cations

in a tetrahedral coordination and is more readily reducible compared to $\alpha\text{-Fe}_2\text{O}_3$. Although this can explain the much lower reduction temperature of Fe_2O_3 in the sol-gel prepared samples, more research is needed concerning the nature of surface iron oxide species in this catalyst. We are in the process of studying these samples with X-ray spectroscopic techniques, EXAFS, XANES, and XPS, which will help resolve the details of their structure.

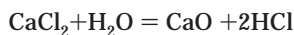
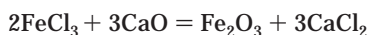
The effect of calcium doping on the catalyst seems to be of a very different nature than modification of the oxidation state or crystalline structure of iron oxide. Since the best improvement of the oxidation properties of 2-MCP is obtained for the samples containing only up to 3% of calcium with respect to the active phase content, it is reasonable to assume a synergistic effect of calcium and iron oxides. TPR profiles of TiFe50Ca3 samples indicate small reducibility changes compared to the TiFe50 sample, i.e., the first peak at 450 °C is slightly shifted toward lower temperature and better developed than the one at 465 °C for TiFe50 sample. Although the changes are visible, they can only partially account for the significant improvement of the catalytic properties of the TiFeCa series in 2-MCP decomposition.

The small shift in reduction peak in TiFeCa may be a result of incorporation of the calcium cation in $\alpha\text{-Fe}_2\text{O}_3$ oxide crystallites. In such a case, since the calcium in CaO has a lower oxidation state than the iron in Fe_2O_3 , to sustain neutrality of the crystal lattice, oxygen vacancies are created. Oxygen vacancies are electron-acceptor sites and can have a localized effect on host cations to be more electron accepting (24).

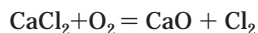
This explanation of Ca effect on TiFe samples is in agreement with the XRD results that indicated the presence of $\alpha\text{-Fe}_2\text{O}_3$ crystallites in both TiFe50 and TiFe50Ca samples. If the concentration of calcium increases above some point, phase separation of CaO and Fe_2O_3 will occur, decreasing the synergistic effect of calcium and iron oxides. As a result, the decrease of catalytic activity of the TiFeCa samples will be observed above certain calcium levels—in fact, such a negative effect of calcium content above 5% has been detected.

Another phenomenon of the calcium effect has to be taken into consideration. Calcium oxide has been previously reported to improve the decomposition of chlorinated hydrocarbons over iron oxide catalysts (10, 11). This effect is attributed to ion exchange between the CaO and FeCl_3 , the latter being formed as a result of interaction of iron oxide with chlorinated hydrocarbons. In this case, calcium serves as a sink for chlorine ions, regenerating iron oxide. Moreover, once CaCl_2 is formed, it was reported to be able to catalyze dechlorination reactions of hydrocarbons more efficiently than the oxide (25). For efficient chloride ion exchange between iron and calcium in an interfacial process, good contact between the phases is necessary. The catalyst systems discussed in the paper cited above were composed of transition-metal ions (Fe, Co) supported on calcium oxide, which ensured interface between the reacting solids. In the case of our system, calcium ions are likely to be incorporated into iron oxide crystallites, which may further improve the ion exchange between the iron and calcium. Once chloride ions are withdrawn from iron by calcium, to maintain the ion exchange efficiency, calcium chloride needs to be reoxidized to CaO. The activation energy for CaCl_2 oxidation by molecular oxygen is low (23 kcal/mol) and even lower in the presence of water vapor (12 kcal/mol) (26), which is a product of the oxidation reaction of hydrocarbons. Thus, CaO is readily regenerated to continue catalyst activity. The stoichiometric interaction between

the calcium oxide and iron chloride can be described as follows:



or



At higher calcium oxide concentrations, however, phase separation of CaO and Fe₂O₃ may occur resulting in lesser contact. Consequently, iron oxide regeneration would have to be completed by gas-phase oxygen. This helps to explain the retardation of the catalyst efficiency with increasing calcium content. Since improvement in catalyst efficiency is only observed at low levels of calcium doping and higher calcium doping results in decreased catalyst efficiency, dechlorination of CHCs by CaO itself is an unlikely explanation for the improved efficiency for 2-MCP destruction observed in our system.

Addition of calcium oxide can also affect the stability of adsorbed species. Alkali dopants have been reported to influence the behavior of oxide catalysts through the stabilization of enolic forms of the ketones on the surface (27), which increases the total oxidation yield. Similarly, addition of calcium into palladium catalyst resulted in stabilization of methoxy species during methanol reaction (24, 28). Generally, since CaO is a basic oxide, it can enhance the adsorption of weak acids such as phenols and contribute to its catalytic destruction.

The best performance of our catalyst was observed for the samples prepared by the sol-gel method doped with small amounts of calcium. The sol-gel method favors the formation of γ -Fe₂O₃ on the surface, which is more readily reduced and thus more active in the MvK process. The admission of calcium in sol-gel samples further increases the amount of γ -Fe₂O₃ formed. TPR profiles presented in Figure 8 reveal a significant increase of the low-temperature reduction peaks attributed to the conversion γ -Fe₂O₃ → Fe₃O₄ and Fe₃O₄ → FeO after introduction of calcium into sol-gel prepared samples. Additionally, after introduction of calcium, the lower temperature peak shifted 40 °C to higher temperature, while the higher temperature peak shifted to lower temperature by 10 °C. These shifts, together with the distinct increase of the intensity of the peaks, indicate structural impacts of calcium doping on iron oxide species.

γ -Fe₂O₃ has a spinel structure with some of the iron ions residing in tetrahedral positions and presence of cationic vacancies. This structure is similar to γ -Al₂O₃, and as such it can be compared to γ -Al₂O₃ transformations. Admission of calcium can result in stabilization of the structure by incorporation of Ca²⁺ ions into cationic vacancies of the oxide, as similarly observed for MgAl₂O₄ (29). As a result, more iron oxide surface species will exist in the form of γ -Fe₂O₃ than in the more thermodynamically stable α form.

Concomitantly, incorporation of calcium ions into cationic vacancies results in the γ -Fe₂O₃ spinel becoming more resistant to reduction. This causes the shift in the TPR reduction peak attributed to the transformation of γ -Fe₂O₃ to Fe₃O₄. Calcium ions may still be present in the crystallites after the transformation into Fe₃O₄ (both oxides have a very similar geometry, with iron in both tetrahedral and octahedral interstitials (30, 31). Thus, the reduction is simplified to removal of some oxygen ligands, without rearrangement of the structure, creating vacancies and perturbation of the lattice. As a result, further reduction to FeO is enhanced.

Oxidation of hydrocarbons according to the MvK mechanism requires involvement of surface lattice oxygen of the

active phase as well as the redox cycle of the cations involved in the oxygen transfer process. In a previous manuscript on the formation of PCDD/F over a copper oxide/silica surface, we demonstrated that electron transfer occurs between the adsorbed molecule and surface cation resulting in the reduction of the latter (32). We believe that this is also occurring in the iron oxide-based catalyst.

Different types of iron oxide species have been attributed to the catalytic activity iron oxides, i.e., α -Fe₂O₃ and FeO (30, 31). We observed correlations between the transition from Fe₃O₄ and FeO oxides in TPR profiles and light-off curves of 2-MCP oxidation. In particular, this is true for the sol-gel prepared samples, where the steep portion of the light-off curves appears at the same temperature as the Fe₃O₄ → FeO transition. Fe₃O₄ has a reverse spinel structure with both Fe²⁺ cations and Fe³⁺ cations, part of the iron(III) having a tetrahedral coordination (31). At the temperature range of the Fe₃O₄ → FeO transformation, reduction of Fe³⁺ is favored. In the presence of gas-phase oxygen, the reverse process also can occur, resulting in redox cycling of iron cations.

Acknowledgments

This research was financially supported under EPA STAR Grant R828191

Literature Cited

- (1) *Interim Emission Standards for 1999 Hazardous Waste Combustor Rule*; EPA530-F-02-008; U.S. Environmental Protection Agency: Washington, DC, 1999.
- (2) Van den Berg, M.; Birnbaum, L.; Bosveld, A. T. C.; Brunström, B.; Cook, P.; Feeley, M.; Giesy, J. P.; Hanberg, A.; Hasegawa, R.; Kennedy, S. W.; Kubiak, T.; Larsen, J. C.; van Leeuwen, F. X. R.; Liem, A. K. D.; Nolt, C.; Peterson, R. E.; Poellinger, L.; Safe, S.; Schrenk, D.; Tillitt, D.; Tysklind, M.; Younes, M.; Wærn, F.; Zacharewski, T. *Environ. Health Perspect.* **1998**, *106*, 775.
- (3) Bonte, J. L.; Fritsky, K. J.; Plinke, M. A.; Wilken, M. *Waste Manage.* **2002**, *22*, 421.
- (4) Yim, S. D.; Koh, D. J.; Nam, I.-S. *Catal. Today* **2002**, *75*, 269.
- (5) Lomnicki, S.; Yeskendir, I.; Xu, Z.; Waters, M.; Amiridis, M. *Organohalogen Compd.* **1999**, *40*, 481.
- (6) Weber, R.; Nagai, K.; Nishino, J.; Shiraiishi, H.; Ishida, M.; Takasuga, T.; Konndo, K.; Hiraoka, M. *Chemosphere* **2002**, *46*, 1247.
- (7) Liu, Y.; Wei, Z.; Feng, Z.; Luo, M.; Ying, P.; Li, C. *J. Catal.* **2001**, *202*, 20.
- (8) Krishnamoorthy, S.; Rivas, J. A.; Amiridis, M. D. *J. Catal.* **2000**, *193*, 264.
- (9) Zhang, Q. W.; Saito, F.; Ikoma, T.; Tero-Kubota, S. *Environ. Sci. Technol.* **2001**, *35*, 4933.
- (10) Decker, S. P.; Klabunde, J. S.; Khaleel, A.; Klabunde, K. J. *Environ. Sci. Technol.* **2002**, *36*, 762.
- (11) Jiang, Y.; Decker, S.; Mohs, C.; Klabunde, K. J. *J. Catal.* **1998**, *180*, 24.
- (12) Doornkamp, C.; Ponec, V. *J. Mol. Catal. A* **2000**, *162*, 19.
- (13) Duma, V.; Hönicke, D. *J. Catal.* **2000**, *191*, 93.
- (14) Lomnicki, S.; Dellinger, B. *Proc. Comb. Inst.* **2002**, *29*, 2463.
- (15) Glisenti, A. *J. Mol. Catal. A* **2000**, *153*, 169.
- (16) Cheng, K.; Dong, L.; Yan, Q. Y.; Chen, Y. *J. Chem. Soc., Faraday Trans.* **1997**, *93*, 2203.
- (17) Barbosa, A. L.; Herguido, J.; Santamaria, J. *Catal. Today* **2001**, *64*, 43.
- (18) Bond, G. C.; Molloy, K. C.; Stone, F. S. *Solid State Ionics* **1997**, *101-103*, 697.
- (19) Nam, S. S.; Kisham, G.; Lee, M. W.; Choi, M. J.; Lee, K. W. *Appl. Organomet. Chem.* **2000**, *14*, 794.
- (20) Halawy, S. A.; Al-Shihry, S. S.; Mohamed, M. A. *Catal. Lett.* **1997**, *48*, 247.
- (21) Suo, Z. H.; Kou, Y.; Niu, J. Z.; Zhang, W. Z.; Wang, H. L. *Appl. Catal., A* **1997**, *148*, 301.
- (22) Kou, Y.; Suo, Z. H.; Niu, H. Z.; Zhang, W. Z.; Wang, H. L. *Catal. Lett.* **1995**, *35*, 279.
- (23) Ennas, G.; Musinu, A.; Piccaluga, G.; Zedda, D. *Chem. Mater.* **1998**, *10*, 495.
- (24) Jackson, N. B.; Ekerdt, J. G. *J. Catal.* **1990**, *126*, 31.
- (25) Mishakov, I. V.; Bedilo, A. F.; Richards, R. M.; Chesnokov, V. V.; Volodin, A. M.; Zaikovskii, V. I.; Buyanov, R. A.; Klabunde, K. J. *J. Catal.* **2002**, *206*, 40.

- (26) Ejima, T.; Kameda, M. *Tohoku Daigaku Senko Seiren Kenkyusho Iho* **1964**, *20*, 29.
- (27) Gandia, L. M.; Gil, A.; Korili, S. A. *Appl. Catal. B* **2001**, *33*, 1.
- (28) Cabilla, G. C.; Bonivardi, A. L.; Baltanas, M. A. *J. Catal.* **2001**, *201*, 213.
- (29) *Catalysis: an Integrated Approach, Second, Revised and Enlarged Edition*; Van Santen, R. A., Van Leeuwen, P. W. N. M., Moulijn, J. A., Averill, B. A., Eds.; Elsevier: New York, 1999; Vol. 123.
- (30) Weiss, W.; Zscherpel, D.; Schlogl, R. *Catal. Lett.* **1998**, *52*, 215.
- (31) Wong, S.-T.; Lee, J.-F.; Cheng, S.; Mou, C.-Y. *Appl. Catal. A: Gen.* **2000**, *198*, 115.
- (32) Lomnicki, S.; Dellinger, B. *J. Phys. Chem. B* **2003**, *107*, 4387.

Received for review November 25, 2002. Revised manuscript received May 15, 2003. Accepted June 18, 2003.

ES026363B